11-1982

Spermidine-Condensed Phi X174 DNA Cleavage by Micrococcal Nuclease: Torus Cleavage Model and Evidence for Unidirectional Circumferential DNA Wrapping.

Kenneth A. Marx
Dartmouth College

Thomas C. Reynolds
Dartmouth College

Proc. Natl. Acad. Sci. USA
Vol. 79, pp. 6484–6488, November 1982
Biochemistry

Spermidine-condensed φX174 DNA cleavage by micrococcal nuclease: Torus cleavage model and evidence for unidirectional circumferential DNA wrapping

(DNA torus/arithmetic DNA band series/topological folding constraints/torus formation mechanism/*in vitro* viral DNA model system)

KENNETH A. MARX AND THOMAS C. REYNOLDS*

Department of Chemistry, Dartmouth College, Hanover, New Hampshire 03755

Communicated by Walter H. Stockmayer, August 2, 1982

ABSTRACT **Spermidine-condensed φX174 replicative form (RF) II DNA was digested with micrococcal nuclease to yield seven identifiable DNA bands forming an arithmetic fragment-length series. The DNA monomer unit length was found to be 780 ± 80 base pairs. This result is most consistent with a proposed model for micrococcal nuclease cleavage of a DNA torus organized by the unidirectional, circumferential wrapping of B-geometry DNA. By a topological consideration, the blunt-end-rod-fusion model for torus formation [Eickbush, T. H. & Moudrianakis, E. N. (1978) *Cell* 13, 295–306] is shown to be inconsistent with our empirical solution results. We propose a continuous, circumferential DNA wrapping model in which a significant fraction of the collapsed circular φX174 RFII DNA molecules form regular toruses comprised of seven complete, unidirectional double-helical wraps.**

Under certain conditions, the interaction of DNA with polyvalent cations, most notably with polyamines, results in a phase transition from the extended DNA solution conformation to compact, close-helix-packed structures (1–9). DNA packaged *in vivo* often results in close-packed structures in which double helices lie roughly parallel, separated by 5–10 Å of solvent. In nucleosomes it has been shown that DNA is helically wound about the histone octamer, resulting in a 28 Å pitch, with adjacent helices some 8 Å apart (10). Double-helical DNA contained within bacteriophage heads is known to be close-packed. Based on x-ray studies, the locally parallel double helices are thought to be separated by about 5 Å of solvent (11). Structural studies on polyamine-condensed DNA have value in that this simple model system may reveal geometric considerations and packing interactions relevant to *in vivo* structures. The polyamine-condensed DNA structures take the form of rods, spheres, toruses, and more complicated intermolecular aggregates, depending on the DNA and polyamine concentrations and specimen preparation procedures. Visualization of these structure shapes by electron microscopy has largely used specimen dehydration protocols, followed by metal shadowing or negative staining (3–7). Recently, freeze-fracture, deep-etch electron microscopy of metal-shadowed, hydrated specimen preparations has revealed similar condensed DNA shapes (1, 2). This result strengthens our view that these DNA structures, in some way, resemble biological structures. One of the predominant geometric forms visualized in polyamine-condensed DNA samples—the torus—represents a simple model for the organization of DNA in double-stranded bacteriophage and virus particles (11–14). Moreover, in measurements on stereomicrographs of Pt-shadowed, hydrated spermidine–DNA toruses, evidence was obtained for the circumferential wrapping of double helix along the torus surface (1). This type of DNA organization, suggested to occur in virus or bacteriophage heads (11–14), has yet to receive solid experimental verification in those systems.

In addition to freeze-fracture electron microscopy, our laboratory has taken a biochemical approach to studying DNA organization in the polyamine-condensed DNA model system. Micrococcal nuclease has been shown to be a valuable probe for structure in these particles, detecting an arithmetic series of broad DNA bands based on the monomer lengths of 760 ± 87 bp in spermidine-condensed calf thymus DNA and 1,003 ± 115 bp in spermidine-condensed bacteriophage λ DNA (unpublished results). These results were successfully interpreted in terms of a model involving regional micrococcal nuclease cleavage of B-geometry DNA forming torus structures by continuous, circumferential wrapping. Circular dichroism (CD) spectroscopy of a similar spermidine-condensed T-7 DNA system has revealed a B-DNA spectrum (15). Because an alternate mechanism has been suggested for torus formation—that is, blunt-end-rod fusion (5)—we undertook to clarify this issue by performing the following experiment. Micrococcal nuclease was used to digest spermidine-condensed φX174 replicative form (RF) II DNA (nicked, circular DNA) and φX174 RF II DNA/*Xho* I digests (linear DNA). The results are topologically inconsistent with torus formation by blunt-end fusion of collapsed DNA rods. We continue to favor a continuous circumferential DNA wrapping model in which a significant fraction of the circular φX174 RF II DNA molecules form regular toruses comprised of seven complete, unidirectional double-helical wraps.

MATERIALS AND METHODS

Spermidine-DNA Condensation and Digestion. The φX174 RF II DNA and φX174 DNA/*Xho* I digests were purchased from New England BioLabs. Spermidine, purchased from Sigma, was used without further purification. The DNA at 10 μg/ml in 1 mM NaCl/10 mM Tris, pH 7.0, was mixed 1:1 (vol/vol) with 2 mM spermidine in the same buffer. This solution containing 5 μg of DNA per ml, 1 mM spermidine, 1 mM NaCl, and 10 mM Tris (pH 7.0) was incubated at 0°C for 3 hr to allow complete spermidine–DNA condensation. Reaction mixtures were then made 1 mM $CaCl_2$, and micrococcal nuclease was added to 5 units/ml. At various time points, aliquots were removed, made 20 mM in EDTA, and frozen. Aliquots were lyophilized and then rehydrated with 50 μl of 30% glycerol.

The publication costs of this article were defrayed in part by page charge payment. This article must therefore be hereby marked "*advertisement*" in accordance with 18 U. S. C. §1734 solely to indicate this fact.

Abbreviations: RF, replicative form; bp, base pair(s); CD, circular dichroism.

* Present address: Stanford University Medical School, Palo Alto, CA 94305.

Gel Electrophoresis. Samples in glycerol were loaded onto a 2% agarose slab gel (Sigma, type I) in 1 mM EDTA/5 mM Na acetate/40 mM Tris, pH 7.8, containing 0.5 μg of ethidium bromide per ml. After electrophoresis at 75 V for 6 hr, the gel was photographed through a no. 23 Wratten filter with Polaroid type 55 film under short-wavelength UV illumination. Molecular weight standards, restriction digests of phage λ DNA with *Hin*dIII and φX174 DNA with *Hae* III (New England BioLabs), were coelectrophoresed to calibrate DNA band sizes.

RESULTS

The φX174 DNA samples, condensed with 1 mM spermidine, were observed to be entirely in the condensed state by virtue of their quantitative sedimentation in a low-speed centrifugation assay (data not shown). DNA fragment distributions resulting from micrococcal nuclease digestion (5 units/ml) of the condensed DNAs are shown in gel electrophoresis photographs (Fig. 1). That discrete, protected DNA-fragment lengths were produced in the course of micrococcal nuclease digestion reflects aspects of the regular DNA organization in the two spermidine-condensed DNA samples.

This banding pattern is a property of every spermidine-condensed DNA so far investigated. For condensed calf thymus, bacteriophage λ, and *Escherichia coli* DNA, micrococcal nuclease digestion produced broad monomer, dimer, and sometimes trimer bands superimposed over significant background DNA fluorescence (unpublished data). When any spermidine-condensed DNA sample was decondensed prior to digestion by the addition of NaCl, an ionic competitor with spermidine for DNA binding, complete absence of the monomer, dimer, and trimer banding pattern was observed. This control experiment clearly associates the banding pattern of Fig. 1 with spermidine-condensed φX174 RF II DNA structures.

There were clearly differences in the two DNA sample series (Fig. 1). The closed circular, nicked φX174 RF II DNA samples (Fig. 1*A*) showed broad but discrete bands, whereas the linear φX174 DNA/*Xho* I samples (Fig. 1*B*) showed broad, poorly resolved peaks. The marked difference in peak resolution between the two identically sized DNA samples probably arises from the difference in their topological states. The φX174/*Xho* I digest has free ends, whereas the circular φX174 RF II DNA has its ends topologically constrained. This constraint must place limits on the condensation pathways available to φX174 RF II DNA, resulting in far more regular condensed structures than for the linear φX174 DNA case. A more regular structure in the condensed DNA, sensed by micrococcal nuclease, would be reflected in the sharper bands seen for circular φX174 RF II DNA.

There are seven identifiable bands in the φX174 RF II DNA sample series in Fig. 1*A*. All seven bands are most visible in the 10-min reaction aliquot. Dots and lines in the 10- and 20-min interlane area mark their exact positions. The band nos. 1–7 were assigned to these intensities. Densitometer tracings of the Fig. 1*A* gel lanes (Fig. 2) clearly identify the seven bands. Similar band features, rather poorly defined, may be noted in Fig. 1*B* lanes for the spermidine-condensed linear φX174 DNA digestion. Also shown in Fig. 2 is a gel tracing from a control experiment in which 0.01 mM spermidine/φX174 RF II DNA (a noncondensing spermidine concentration) was digested with micrococcal nuclease. Because no evidence of bands was seen, the occasional DNA sequence specificity reported for micrococcal nuclease cannot play a role in the origin of the banding sequence (16, 17).

A major fraction of the DNA fluorescence intensity in Figs.

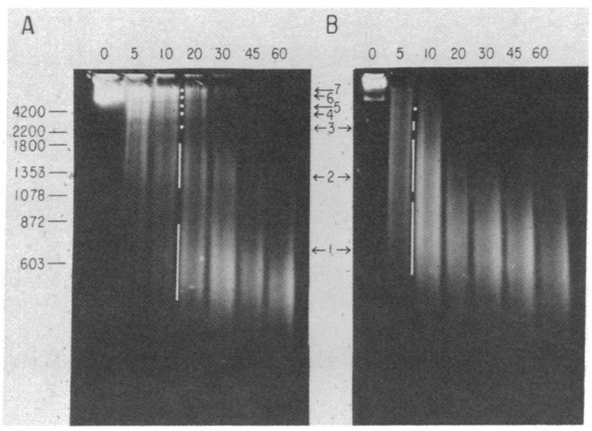

FIG. 1. Agarose gel electrophoresis of micrococcal nuclease digests of spermidine-condensed φX174 DNA. (*A*) RF II nicked, circular form. (*B*) Linear (*Xho* I digest) form. The DNAs were condensed with spermidine, digested with micrococcal nuclease for the times indicated (min), and electrophoresed in a single 2% agarose gel. In *A* for calibration purposes, restriction enzyme-digested DNA fragment positions and sizes in bp are indicated on the left, and the positions of seven distinct DNA bands in the φX174 RF II DNA samples are indicated with white dots and lines. The numbered arrows identify the seven bands and their equivalent positions in *A* and *B*.

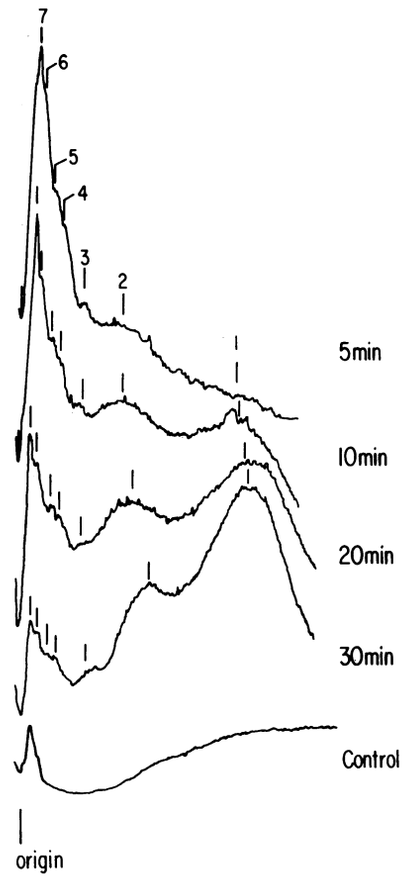

FIG. 2. Densitometer tracings of DNA fragment distributions. Micrococcal nuclease digestion aliquots of 1 mM spermidine-condensed φX174 RF II DNA, electrophoresed in Fig. 1, were photographed, and the negative was traced in a Helena Quick-scan R & D Densitometer. The bottom densitometer trace (control) is from a photographic negative of a 1.5% agarose gel in which aliquots of micrococcal nuclease (1 unit/ml) digests of 0.01 mM spermidine/φX174 RF II DNA were electrophoresed; 0.01 mM spermidine is noncondensing. An aliquot taken at 30 sec is shown.

1A and 2 occurred in the seven-band sequence. This suggests that a significant fraction of the circular ϕX174 RF II DNA in the sample was condensed into structurally similar particles. Moreover, there appeared to be a precursor–product relationship between the highest molecular weight bands and succeeding lower molecular weight bands. That is, the fluorescence intensity of the higher-number bands disappeared concomitant with the appearance of DNA fluorescence intensity in successively lower-number bands, suggesting the production of lower molecular weight bands from the higher molecular weight bands by micrococcal nuclease cleavage. Eventually, all of the fluorescence intensity resided in band no. 1. We showed in related systems that DNA of this size was subsequently degraded by micrococcal nuclease to low molecular weights (unpublished data). The precursor–product relationship of the seven DNA bands is further proof that the spermidine-condensed ϕX174 RF II circular DNA particles form a relatively homogeneous population of structures. By contrast, the spermidine-condensed ϕX174/*Xho* I linear DNA particles, although showing a precursor–product relationship between DNA bands, must be considerably more heterogeneous in structure.

Micrococcal nuclease shows exonucleolytic-like cleavage of DNA condensed in chromosomal systems (18, 19). We noted an effect similar to this in digesting spermidine-condensed calf thymus DNA particles (unpublished data). Exonucleolytic cleavage was evident (here in Fig. 1 and 2) in the progression of the labeled peaks, especially nos. 1 and 2, to smaller average sizes. We decided to correct for exonucleolytic cleavage, so that our interpretation of the digestion data reflected the original particle DNA structure sensed by micrococcal nuclease. Midpoints of peaks 1, 2, and 3 in Fig. 1, determined from the two sets of marker fragments, are plotted in Fig. 3 against digestion time. The progression in peak midpoints can be seen in this data, and a smooth curve through the data has been used to estimate the zero-digestion-time extrapolated peak midpoints. These values, tabulated in Table 1, represent the DNA sizes that result primarily from the initial endonucleolytic cleavage of particle DNA by micrococcal nuclease.

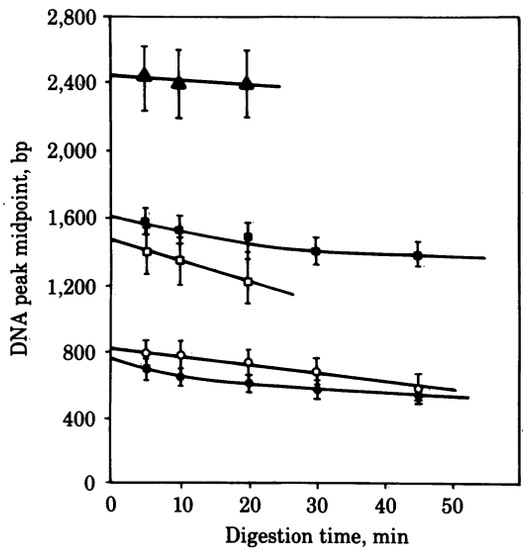

FIG. 3. DNA peak sizes as a function of digestion time. The estimated DNA band midpoints from the Fig. 1 gel are plotted against the time of micrococcal nuclease digestion for ϕX174 RF II DNA circular bands 1 (●), 2 (■), and 3 (▲) and for ϕX174/*Xho* I linear bands 1 (○) and 2 (□). Uncertainties in peak midpoint determination are reflected in the error bars about each data point. The curves are not fit to the data but simply connect the points.

The most striking aspect of the results in Table 1 is the peak midpoint ratios. Relative to the band 1 size for each digested DNA, higher band sizes fall into an arithmetic series. This is most obvious in the data from the more homogeneous particle distribution of spermidine-condensed ϕX174 RF II circular DNA. Here, the first three bands have a near-perfect arithmetic-size relationship. Band no. 4 is somewhat larger than expected; however, its real size could only be roughly estimated from the agarose gel in Fig. 1.

DISCUSSION

Torus Cleavage Model Generates Arithmetic DNA Band Series. Manning has successfully described the spermidine-condensed ϕX174 RF II DNA phenomenon in terms of counterion condensation theory (20). Torus shaped spermidine–ϕX174 RF II DNA complexes represent simple and important *in vitro* model systems for the organization of condensed DNA in certain bacteriophage and viruses (11–14). Therefore, it is imperative that the arithmetic DNA fragment series produced here by micrococcal nuclease digestion be rationalized in terms of a model for the organization of spermidine-condensed ϕX174 DNA. The majority of electron microscopy and supporting studies point to toruses as the predominant regular structures present in these preparations. For this reason, we have developed a micrococcal nuclease cleavage model based on the torus geometry (Fig. 4). We assume circumferential DNA wrapping to form the model torus, having already presented evidence for circumferential winding of putative calf thymus DNA double helices from a parallax bar analysis of high-resolution stereomicrographs of spermidine–calf thymus DNA toruses in preparations similar to these (1, 2). Moreover, we made similar observations in spermidine–condensed ϕX174 RF II DNA torus preparations (unpublished data). With this simple circumferential torus organization, *our micrococcal nuclease cleavage model may be summarized as follows.*

(*i*) Double-stranded DNA cleavage by micrococcal nuclease anywhere on the torus surface is kinetically slow because of the inaccessibility of each DNA double helix in the hexagonally close-packed array.

(*ii*) In the region of a double-strand cleavage, successive dou-

Table 1. DNA band sizes and band size ratios from micrococcal nuclease-digested spermidine-condensed ϕX174 DNA samples*

DNA	Band no.	Extrapolated size, bp	Extrapolated size ratio†
ϕX174 RF II (nicked, circular, 5,386 bp)	1	780 ± 80	1.0
	2	1,580 ± 150	2.0
	3	2,450 ± 250	3.1
	4	(3,400)	(4.4)
	5	—	—
	6	—	—
	7	—	—
ϕX174/*Xho* I digest (linear, 5,386 bp)	1	830 ± 120	1.0
	2	1,470 ± 250	1.8
	3	—	—
	4	—	—

* Based upon zero-digestion-time extrapolated values from Fig. 2. Uncertainty in the extrapolated values is only an estimate based upon the uncertainties in each data point and the unknown curve shape in the low-time regions of the Fig. 3 curves.

† This size ratio is determined by dividing the extrapolated size for each band by the appropriate band 1 extrapolated size.

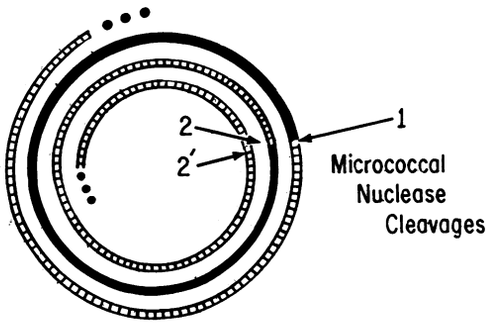

FIG. 4. Two-dimensional representation of a spermidine-condensed DNA torus cleavage model in cross-section. In this structure DNA is circumferentially wrapped in a unidirectional fashion. Assume that in any given DNA double helix, there is, in three dimensions, hexagonal close-packing of nearest neighbor double helices. The consequence of micrococcal nuclease cleavages 2 and 2′ after the first cleavage event (arrow 1) can be seen to generate two discrete fragment lengths of DNA. Cleavage 2 generated a monomer fragment with a length of one torus circumference (solid section in diagram). Cleavage 2′ generates a dimer fragment with a length of two torus circumferences. Because of hexagonal DNA packing in three dimensions, the nearest neighbors to the initial cleavage strand, if cleaved second, would result in an arithmetic series with members well above dimers of the torus circumference length.

ble-stranded micrococcal nuclease cleavages in nearest-neighbor double helices is kinetically fast.

The consequence of these two digestion principles acting upon a three-dimensional, hexagonally close-packed DNA torus structure is to generate an arithmetic series of DNA fragment lengths, the monomer unit being one torus circumference. To illustrate this in two dimensions (Fig. 4), the first cleavage event, kinetically slow, is shown to occur at arrow 1. The second cleavage event can occur anywhere else on the torus at a slow rate but occurs rapidly in the vicinity of the first cleavage event. Therefore, if cleavage occurs at arrow 2 on the nearest-neighbor helix section shown, a monomer torus circumference length has been generated—arrow 1 to arrow 2 (blackened helix section). If cleavage occurs at arrow 2′ (in three dimensions, this could be a nearest-neighbor double helix), then a dimer torus circumference length has been generated—arrow 1 to arrow 2′. Extending this approach to a three-dimensional torus with hexagonal DNA packing allows for the generation of higher members of the torus circumference arithmetic series.

The circumferential DNA wrapping model fits our spermidine-condensed ϕX174 RF II DNA digestion data extremely well. We can clearly identify seven DNA bands in the arithmetic series based on a 780-bp monomer length. Given our model, there must be seven DNA wraps or 7(780) = 5,460 bp of total DNA. This is close to the known size of ϕX174 RF II DNA (5,386 bp). We have performed a preliminary freeze-fracture electron microscopic examination of the spermidine-condensed ϕX174 RF II DNA preparation. From a series of 27 non-tilt corrected torus monomer (one ϕX174 RF II molecule) circumference measurements, we have determined the average DNA circumference at the midpoint of the torus ring to be about 725 ± 70 bp (unpublished data). This measured value, lower than the real value, is in good agreement with the monomer length of 780 ± 80 bp measured in our micrococcal nuclease digestion study and proposed to wrap circumferentially once about the torus.

For the purpose of exposition, our model assumes a particular DNA geometry—the B form. Although we have not determined the CD spectrum of our spermidine-condensed ϕX174 RF II DNA preparation, spermidine-condensed T-7 DNA under solution conditions similar to those in this study revealed a B form CD spectrum (15).

Topological Considerations and Torus Model Discrimination. In our discussion of the micrococcal nuclease digestion of spermidine-condensed ϕX174 RF II DNA, we presented a cleavage model based on a torus comprised of unidirectional circumferentially wrapped DNA. Although this model (here model 1) can quite easily explain the arithmetic series of DNA fragment lengths, it remains a nonunique explanation. It has been proposed that spermidine–DNA toruses may form by a mechanism (blunt-end-rod fusion) in which DNA collapses into a rod, which then bends and fuses its ends, thereby forming a torus (5).

The two torus models and their formation pathways are indicated schematically in Fig. 5 for the circular ϕX174 RF II DNA case. It can be seen that model 2 (blunt-end-rod fusion) yields a structure very similar to model 1. The major distinctions in model 2 are the existence of rod ends and the alternating direction of the circumferentially wrapped DNA. As noted above, Model 2 also can be used to explain an arithmetic series

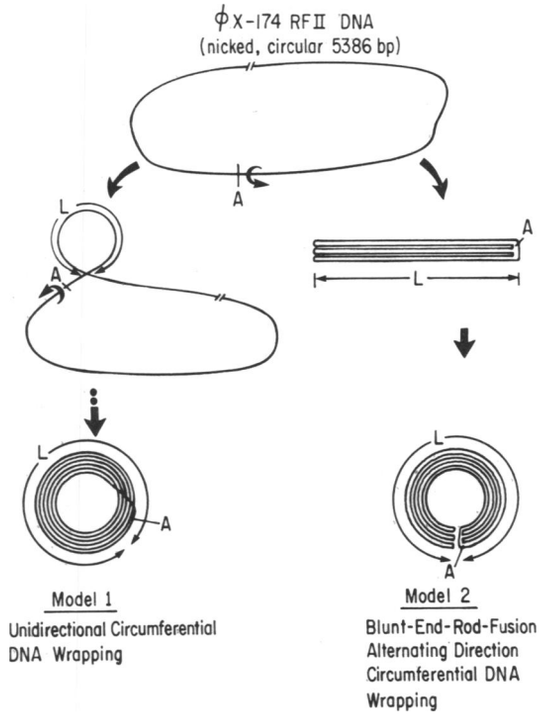

FIG. 5. Topology of two simple circumferentially wrapped DNA torus models. The DNA (a single solid line for the purpose of clarity) used to illustrate these cases is ϕX174 RF II DNA, a double-helical DNA that is circular (5,386 bp) and has one single-stranded nick at reference point A. The arrow indicates that super-helical turns may be introduced into the molecule at this point. In the model 1 pathway, where DNA is wrapped circumferentially in a continuous unidirectional fashion, superhelical turns are introduced into the ϕX174 RF II DNA to fold it into the condensed regular torus. The torus circumference length L divided into 5,386 bp will give n—the number of complete DNA wraps. In this model, n must be an integer because the DNA is circular; but it can be any integer. The case $n = 6$ is illustrated here. Model 2 pathway has the ϕX174 RF II DNA folding initially into a rod-like structure of length L, which then bends to fuse its blunt ends, resulting in a torus of circumference L. In this model, every deposition of length L DNA on the rod must be accompanied by deposition of a subsequent length L DNA segment in the opposite direction. This is necessary because the molecule is circular and must ultimately come back to the origin (for example, reference point A) to complete the circle. Hence, n (5,386 bp per length L) is constrained to always be an even integer. The case $n = 6$ is illustrated here.

of DNA fragment lengths upon micrococcal nuclease cleavage. Double-stranded DNA cleavage at the end regions where DNA is sharply bent can be seen to produce this arithmetic DNA fragment series result, again based on the torus-circumference-length monomer unit.

Thus, is it possible to discriminate empirically between these two very different torus organization models? After all, the two models may be indistinguishable electron microscopically under certain conditions and may both form an arithmetic DNA fragment series upon micrococcal nuclease digestion. Consideration of the torus n,L pair parameters (n is the number of circumferential wraps; L is the DNA circumferential wrap length) for the two models does allow us to discriminate unambiguously between them (see Table 2). It will be noted that in both models n must be an integer. This is required topologically because we are collapsing a circular DNA molecule. However, the crucial difference in the two models is that n can be any integer and satisfy model 1, while n is constrained to even integers only to satisfy model 2. This can be visualized most easily in the following way. For model 1, the topological end closure can be maintained every time the DNA strand makes one complete circumferential wrap of the torus. In model 2, the topological end closure must be maintained by the DNA strand making two circumferential torus wraps of opposite direction or, when viewed at the intermediate rod stage, by an L length of DNA strand lying down in one direction (e.g., from A going left on the rod in Fig. 5) followed by an equivalent L length of DNA strand lying down in the opposite direction (e.g., from the left end of the rod back to A).

The consequence of the n value constraints for models 1 and 2 are summarized in Table 2. Of course, the particular integer value of n fixes a value for L as shown. Model 1 can be seen to satisfy the three n,L pairs listed (only these three are of interest to us), whereas model 2 can only satisfy the $n = 6$ or 8 situation. Model 2 is topologically incapable of producing an $n = 7$ torus geometry. Although $n = 6$ or $n = 8$ geometry toruses can help to give rise to the broad peaks noted in the Fig. 1 gel, it will be recalled that the statistical situation $n = 7$, $L = 780 \pm 80$ bp is predominant experimentally for the spermidine-condensed circular ϕX174 RF II DNA system. Therefore, these experimental data cannot be explained by the model 2 blunt-end-rod-fusion torus, as has been proposed (5). We feel that the blunt-end-rod-fusion mechanism may provide a thermodynamic pathway available for DNA condensation and some torus formation only under certain conditions of low water activity. In our freeze-fracture experiments, we see no hydrated specimens resembling rod-like DNA structures of any length L at all close to the torus circumference lengths measured for spermidine-condensed ϕX174 RF II or calf thymus DNAs (refs. 1 and 2; unpublished data).

Table 2. Torus model parameters for condensed circular ϕX174 RF II DNA

n	L, (5,386/n bp)	Model 1	Model 2
6	898	+	+
7	770	+	−
8	670	+	+

For the relevant indicated values of n, the corresponding required value of L has been calculated. The last two columns indicate whether the two torus models can accommodate the n,L pair values; $n = 7$ and $L = 780$ bp are our experimentally determined value pair, within the context of our micrococcal nuclease cleavage model for the torus.

We take the above topological argument and our electron-microscope observations as further indication that in aqueous solution something like model 1 unidirectional circumferential DNA wrapping is the predominant way in which toruses are formed by condensing DNA. By no means have we proved that model 1 is the solution condensation mechanism. However, it remains to us the most attractive, physically simple model by which all of our biochemical and electron microscopic data may be explained.

This investigation was supported by Biomedical Research Support Grant RR-05392 from the Biomedical Research Support Branch of the National Institutes of Health's Division of Research Facilities and Resources and National Institutes of Health Grants GM 25886-02 and AI 17586-01. Additional support is acknowledged from a Research Corporation Grant 8859.

1. Ruben, G. C., Marx, K. A. & Reynolds, T. C. (1981) in *Proceedings of the 39th Meeting of the Electron Microscope Society of America, Atlanta, GA*, ed. Bailey, G. W. (Claitor's, Baton Rouge, LA), pp. 438–439.
2. Ruben, G. C., Marx, K. A. & Reynolds, T. C. (1981) in *Proceedings of the 39th Meeting of the Electron Microscope Society of America, Atlanta, GA*, ed. Bailey, G. W. (Claitor's, Baton Rouge, LA), pp. 440–441.
3. Chattoraj, O. K., Gosule, L. C. & Schellman, J. A. (1978) *J. Mol. Biol.* **121**, 327–337.
4. Skuridin, S. G., Kadykov, V. A., Shashkov, V. S., Evdokimov, Yu. M. & Varshavski, Ya. M. (1978) *Mol. Biol. (Moscow)* **12**, 413–420.
5. Eickbush, T. H. & Moudrianakis, E. N. (1978) *Cell* **13**, 295–306.
6. Widom, J. & Baldwin, R. L. (1980) *J. Mol. Biol.* **144**, 431–453.
7. Allison, S. A., Herr, J. C. & Schurr, J. M. (1981) *Biopolymers* **20**, 469–488.
8. Wilson, R. W. & Bloomfield, V. A. (1979) *Biochemistry* **18**, 2192–2196.
9. Mandelkern, M., Dattagupta, N. & Crothers, D. M. (1981) *Proc. Natl. Acad. Sci. USA* **78**, 4294–4298.
10. Finch, J. T., Lutter, L. C., Rhodes, D., Brown, R. S., Rushton, B. & Klug, A. (1977) *Nature (London)* **269**, 29–36.
11. Earnshaw, W. C. & Casjens, S. R. (1980) *Cell* **21**, 319–331.
12. Klimenko, S. M., Tikchonenko, T. I. & Andreev, V. M. (1967) *J. Mol. Biol.* **23**, 523–533.
13. Furlong, D., Swift, H. & Roizman, B. (1972) *J. Virol.* **10**, 1071–1074.
14. Richards, K. E., Williams, P. C. & Calendar, R. (1973) *J. Mol. Biol.* **78**, 255–259.
15. Gosule, L. & Schellman, J. A. (1978) *J. Mol. Biol.* **121**, 311–326.
16. Ponder, B. A. J. & Crawford, L. V. (1977) *Cell* **11**, 35–49.
17. Fittler, F. & Zachau, H. G. (1979) *Nucleic Acids Res.* **7**, 1–13.
18. Noll, M. (1974) *Nature (London)* **251**, 249–251.
19. Lohr, D., Corden, J., Tatchell, K., Kovacic, R. T. & Van Holde, K. E. (1977) *Proc. Natl. Acad. Sci. USA* **74**, 79–83.
20. Manning, G. S. (1978) *Q. Rev. Biophys.* **11**, 179–246.